RESEARCH PAPER

PCCP
www.rsc.org/pccp

DFT plane wave calculations of the atomic and electronic structure of $LaMnO_3$ (001) surface

E. A. Kotomin,*[ab] R. A. Evarestov,[c] Yu. A. Mastrikov[a] and J. Maier[a]

[a] *Max Planck Institute for Solid State Research, Heisenbergstr. 1, D-70569 Stuttgart, Germany. E-mail: kotomin@fkf.mpg.de, j.mastrikovs@fkf.mpg.de, weiglein@fkf.mpg.de; Fax: +49 711 689 1722*

[b] *Institute for Solid State Physics, University of Latvia, Kengaraga str. 8, Riga LV-1063 Latvia. E-mail: kotomin@latnet.lv; Fax: +371 713 2778*

[c] *Department of Quantum Chemistry, St. Petersburg University, 198504 St. Peterhof, Russia. E-mail: evarest@hm.csa.ru; Fax: +007 812 4286939*

Received 4th March 2005, Accepted 12th April 2005
First published as an Advance Article on the web 25th April 2005

We present the results of *ab initio* DFT plane wave periodic structure calculations of the $LaMnO_3$ (001) surface. The effects related to three different kinds of pseudopotentials, the slab thickness, magnetic ordering, and surface relaxation are studied and discussed. The antiferromagnetic surface lowest in energy (that is, the spins on Mn ions are parallel in basal plane and antiparallel from plane to plane) has a considerable atomic relaxation up to the fourth plane from the surface. The calculated (Bader) effective charges and the electronic density maps demonstrate a considerable reduction of the Mn atom ionicity on the surface accompanied by a covalent contribution to the Mn–O bonding.

1. Introduction

Sr-doped $LaMnO_3$ (LMO) attracts great attention as a cathode material for solid oxide fuel cells[1] as well as because of its bulk magnetic properties.[2–5] Surprisingly, LMO *surface properties* have been studied very little, especially theoretically. To our knowledge, there exist only a few surface structure calculations for manganese perovskites; LSDA study refers to $CaMnO_3$ and $La_{1/2}Ca_{1/2}MnO_3$ (100) surfaces in their non-cubic modifications[6] whereas our LMO studies of the LMO (110) surfaces involve both classical shell model[7–9] and *ab initio* Hartree–Fock (HF) calculations.[10,11] In the latter papers, the results of the first HF calculations for the unrelaxed (001) surface were reported.

Ab initio calculations of the bulk LMO electronic structure were performed earlier in the HF LCAO approximation[2,3] and using the relativistic full-potential-GGA LAPW.[4] In these calculations several different crystalline structures were considered. The ideal perovskite (cubic) structure with five atoms (one formula unit) per a primitive unit cell (Fig. 1a), is stable above 750 K, with the experimental lattice constant $a_0 = 3.95$ Å. The UHF LCAO calculations[3] gave the optimised lattice constant very close to this experimental value. In the UHF calculations[2] the tetragonal structure, consisting of $\sqrt{2} \times \sqrt{2} \times 2 = 4$ primitive unit cells of the undistorted perovskite structure, was assumed. For such a structure, it was found, in both HF and LSDA approximations, that the ground state of LMO is ferromagnetic (FM, spins of all 4 Mn atoms in a supercell are parallel).

The low-temperature LMO structure is orthorhombic (comprising four formula units, space group *Pbnm*, Fig. 1b). The experimental values of the lattice parameters $a = 5.532$ Å, $b = 5.742$ Å, $c = 7.668$ Å, can be compared with $a = b = 5.582$ Å, $c = 7.894$ Å for the above mentioned tetragonal structure containing four formula unit cells, and the experimental value of the cubic lattice constant $a_0 = 3.95$ Å. The difference in these two sets of structure parameters arises due to strong Jahn–Teller (JT) distortions of the MnO octahedra and their rotations (this effect is known as MnO_6 octahedra tilting). For the orthorhombic structure, HF, LSDA calculations,[2,3] as well as LAPW[4] predict the LMO ground state to be an antiferromagnetic (AFM) insulator, in agreement with the experiment. The calculated energy of this state is lower than for the FM state, by 1.055 eV per Mn in the HF calculation and 0.156 eV per Mn in the LSDA calculation.[2] This demonstrates a strong dependence of the FM–AFM energy difference on the calculation scheme. The orthorhombic lattice parameters optimised in HF calculations[3] are $a = 5.620$ Å, $b = 5.740$ Å, $c = 7.754$ Å. Corresponding to these parameters the "virtual" cubic structure has the lattice constant $a_0 = \frac{1}{2\times3}(a\sqrt{2} + c + b\sqrt{2}) = 3.97$ Å. (The latter value is obtained by averaging over the orthorhombic lattice parameters.) Along with the lattice parameter optimisation, to our knowledge there exists only a single study on the UHF optimisation of the local atomic coordinates *inside* the orthorhombic unit cell.[3] The UHF method was also successfully used for calculating the magnetic coupling constants in LMO.[12] It was shown that the magnetic coupling constants depend considerably on the hybrid functional used.

In this paper, we present the results of detailed *ab initio* calculations for the LMO (001) polar surface with emphasis on its relaxation for different magnetic configurations. Its MnO_2 termination could be important for fuel cell applications, in which adsorption of O_2 might occur, followed by its ionization, dissociation and ion transfer in the electrolyte. In order to check results obtained by means of the UHF, we performed DFT generalized gradient approximation (DFT–GGA) plane wave calculations which also permit considerably faster structure optimisation. In Section 2 we discuss basic results for the bulk properties of LMO, which serve as a test of the method ability to calculate the atomic and electronic structure of ABO_3 perovskites. The results of surface calculations are presented in Section 3. We analyse how the results depend on the different kinds of pseudopotentials, the slab thickness, and magnetic ordering. Special attention is paid to the surface relaxation.

DOI: 10.1039/b503272e

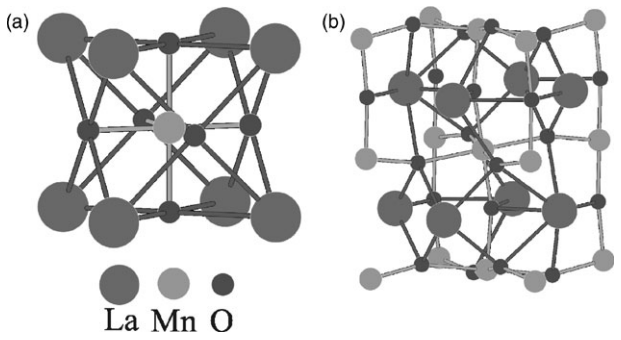

Fig. 1 Ideal perovskite cubic (a) and relaxed orthorhombic (b) structure.

2. Bulk $LaMnO_3$ calculations

For calculations we employed the *ab initio* DFT plane wave based computer code VASP.[13,14] The GGA–Perdew–Wang-91 potential was used for exchange–correlation.[16] We checked results for three types of the projector augmented-wave pseudopotentials for the inner electrons (referred hereafter as PP-1,2,3)—La, Mn, O; La, Mn_{pv}, O_s; and La, Mn_{pv}, O, where the lower index pv means that Mn 3p states are treated as valence states, and s means soft pseudopotentials with reduced cut-off energy and/or reduced number of electrons (Table 1). The typical plane wave cut-off energy was $E_{cut} = 600$ eV. We used the Monkhorst–Pack scheme[17] for ***k***-point mesh generation, which was typically 4 4 4 (if not otherwise stated).

Depending on the four Mn spin orientations in the orthorhombic unit cells of 20 atoms, there are four possible magnetic orderings: ferromagnetic (FM, all spins are parallel), as well as A-, G-, and C-type antiferromagnetic (AAF, GAF, CAF). In the AAF case the Mn spins are parallel in basal plane and antiparallel from plane to plane; in the GAF each nearest neighbour pair of Mn spins are antiparallel, and in the CAF each nearest neighbour pair of Mn spins are antiparallel in the basal plane and parallel along the z axis. (We neglect in this paper the fifth option of the ferrimagnetic ordering where the spin of one of the four Mn atoms in the cell is antiparallel to those of the other three.) Neglect of spins on Mn atoms corresponds to the non-magnetic (NM) state. The ground state electronic configuration of a single Mn^{3+} ion is $t_{2g}^3 e_g^1$ (all four electrons have the same spin projection, *i.e.* a high spin state). The VASP code calculates magnetic moments on atoms which do not necessarily coincide with the initial guess.

Table 2 shows the optimised cubic (high temperature) lattice constants for three possible magnetic states, three kinds of pseudopotentials, and two cut-off energies. As one can see, an increase of the cut-off energy from 269.9 eV up to 600 eV increases the lattice constant only by 0.01–0.02 Å. In all cases the optimised lattice constant is smaller than the experimental one. The closest agreement is observed for the FM magnetic ordering and PP-2 pseudopotentials. The optimised magnetic moments on Mn atoms are close to the expected $\pm 4\ \mu_B$. The results for PP-3 potentials are quite similar to those of PP-2, however, the latter are computationally much less costly. This is why we used PP-2 pseudopotentials in the surface calculations. Table 3 gives the cohesive energies E_0 calculated using three types of pseudopotentials. The cohesive energies were calculated as the difference of the VASP unit cell total energy and the sum of the atomic energies of the constituent atoms. The analysis for relaxed and unrelaxed cubic unit cells shows that the cohesive energies for the PP-1 exceed by 10–20% the experimental value of 30.3 eV, whereas those calculated using the PP-2 and PP-3 are in very good agreement with the experiment.

Table 1 Projector-augmented wave (PAW), generalized gradient approximation (GGA) pseudopotentials (PP) used in these calculations[14]

Pseudopotential	Cut-off energy/eV	No. of valence electrons	Valence electrons
La	219.044	11	5s2 5p6 6s2 5d1 (4f)
Mn	269.944	7	4s1 3d6
Mn_{pv}	269.887	13	3p6 4s1 3d6
O	400	6	2s2 2p4
O_s	250	6	2s2 2p4

Table 2 Optimised lattice constants for a cubic unit cell (in Å). The experimental value is 3.95 Å, the ***k***-set is 4 4 4, PP-1, PP-2 and PP-3 correspond to three types of pseudopotentials—La, Mn, O; La, Mn_{pv}, O_s; and La, Mn_{pv}, O—see explanation of the pseudopotentials and magnetic structures PM, FM and AAF in the text. The relevant unit cells contain 5, 5 and 10 atoms, respectively

PP	PP-1		PP-2		PP-3	
E_{cut}/eV	269.9	600	269.9	600	269.9	600
NM	3.745	3.751	3.821	3.837	3.815	3.827
FM	3.763	3.772	3.887	3.919	3.887	3.917
AAF	3.778	3.791	3.882	3.916	3.880	3.908

Table 4 presents three optimised lattice parameters of the low-temperature orthorhombic phase and the cohesive energies for five different magnetic orderings. The atomic coordinates in the unit cell were fixed according to the experimental data.[15] In agreement with the experiment, the lowest energy corresponds to the AAF structure. The optimised a and b lattice parameters are also close to the experimental values; the c parameter differs from the experiment by 0.05 Å. Recent calculations[12] based on UHF and several hybrid functionals also suggest a similar energetic ranging of the magnetic structures: AAF < GAF < CAF. The results of our atomic coordinate optimisation inside the unit cell with fixed lattice parameters are summarized in Table 5. One can see that the calculated AAF structure is very close to the experimental one, while the difference between the AAF and FM structures is small.

Lastly, Table 6 presents the results of *simultaneous* optimisation of the lattice parameters and atomic coordinates in the orthorhombic unit cell using four different magnetic ordering. In contrast to the experimentally observed ground state, the AAF structure in our calculations is higher in energy than the FM structure, however the difference (0.06 eV per Mn atom) lies in the limits of the method accuracy. Based on these results, we can conclude that the DFT–GGA plane wave calculation reliably reproduces the low-temperature experimental structure of the bulk LMO.

3. The (001) surface calculations

Note that in fuel cell applications, the operational temperature is so high ($T > 800$ K) that the LMO unit cell is cubic,[4,5] and thus JT lattice deformation around Mn ions and related magnetic and orbital orderings no longer take place. Of primary interest for fuel cell applications are the LMO surface properties, *e.g.* the optimal positions for oxygen adsorption, its surface transport properties, as well as the charge transfer behaviour. Moreover, the relaxed surface energies for LMO (001), as we show below, are about 1 eV, *i.e.* larger than the JT energy in LMO,[5] and the magnetic exchange energy (10^{-2} eV). Periodic *ab initio* calculations of the crystalline surfaces are usually performed considering the crystal as a stack of planes perpendicular to the surface, and cutting out a 2D slab of the finite thickness but periodic in x, y plane. As the plane wave calculations require the translational symmetry in all three dimensions, the 2D slab is repeated periodically along the z axis (Fig. 2). The so-called *vacuum gap* is by definition the

Table 3 The cohesive energies E_0 (in eV) for cubic structures as in Table 2, for the experimental lattice constant (3.95 Å), the relaxation energies E_{rel} and ΔE, due to lattice constant optimisation. The experimental estimate of the cohesive energy is 30.3 eV

	PP-1						PP-2						PP-3					
	269.9			600			269.9			600			269.9			600		
	E_0	E_{rel}	ΔE	E_0	E_{rel}	ΔE	E_0	E_{rel}	ΔE	E_0	E_{rel}	ΔE	E_0	E_{rel}	ΔE	E_0	E_{rel}	ΔE
NM	33.99	35.02	1.03	34.55	35.43	0.88	29.66	30.06	0.40	29.59	29.85	0.26	29.91	30.31	0.40	30.46	30.74	0.28
FM	34.85	35.51	0.65	35.41	35.92	0.51	30.70	30.78	0.09	30.62	30.64	0.02	30.94	31.03	0.08	31.49	31.51	0.02
AAF	34.83	35.40	0.57	35.39	35.82	0.43	30.66	30.76	0.10	30.59	30.61	0.03	30.91	31.01	0.10	31.45	31.48	0.03

difference between the length of z axis oriented translation vector and the slab thickness. We used for the vacuum gap the value of 15.8 Å. In our calculations, we used stoichiometric $LaO\cdots MnO_2$ slabs of different thicknesses, varied from 4 to 12 planes. These slabs were built of the cubic unit cells where all atoms were allowed to relax along the z axis to reach the minimum of the total energy. In some calculations we also optimised the lattice parameters a, b of the surface square unit cell. The surface energy was calculated according to ref. 11:

$$E_s = \frac{1}{2}(E_{slab} - nE_{bulk}), \quad (1)$$

where E_{slab} is the total energy of the stoichiometric slabs with MnO_2 and LaO terminations, E_{bulk} the bulk energy per unit cell, and n the number of formula units in a slab (half the number of planes in a slab). When calculating the surface energy for *relaxed* slabs, we used as the reference the bulk unit cell energies calculated for the relaxed cubic cells (Table 3).

In Table 7 we compare the results for the unrelaxed and relaxed surface energies for the PP-2 pseudopotentials, NM (spins are neglected, closed shell calculations), FM and AAF (half Mn ions in a slab have spins up, another two spins down) magnetic orderings. First of all, the AAF magnetic structure, which mimics the disordered spin orientations at high temperatures, is always lower in energy than the NM structure where spins on Mn ions are neglected. The typical energy difference is as large as $\sim$1 eV per Mn atom. In contrast, the FM and AAF configurations are very close in energy. Secondly, the cleavage (unrelaxed) surface energy is almost constant, independent on the slab thickness. However, surface relaxation reduced this energy down, by a factor of about two, similarly for the FM and AAF magnetic structures. The relaxed surface energies show a monotonic but very slight increase with the slab thickness, up to 0.89 eV for 12-plane AAF slab. This value is close to that found in our recent HF calculations[11] and even smaller than the energy for the O-terminated (110) surface.[7,11] This means that the (001) surface is energetically favorable and thus MnO termination could play an important role in fuel cell and other applications. Thirdly, when the on-plane structure relaxation is also allowed, the optimised lattice parameters a, b in both cases are smaller than the experimental value, as it occurs also in the bulk calculations (Table 2). The calculated surface energy for the FM configuration differs from that for the AAF by no more than $\sim$0.02 eV unit cell^{-1}. In order to compensate the dipole

Table 4 Optimization of lattice constants (in Å) with fixed experimental positions of atoms inside the orthorhombic unit cell of 20 atoms (Table 5)

	a	b	c	Cohesive energy/eV cell^{-1}
Experimental[15]	5.7473	7.6929	5.5367	30.3
NM	5.5285	7.6434	5.5610	29.77
FM	5.7102	7.8063	5.5891	30.84
AAF	5.7661	7.7077	5.5876	30.86
GAF	5.8071	7.6544	5.5628	30.78
CAF	5.7296	7.7927	5.5472	30.79

Table 5 Optimised fractional coordinates of atoms in the orthorhombic unit cell. The lattice parameters a, b, c are taken from experimental data (Table 4). E_{cut} = 600 eV, the ***k***-set is 4 2 4. Mn coordinates are (1/2, 0, 0)

		a	b	c	Cohesive energy/eV cell^{-1}
Experimental[15]	La	0.0490	0.25	0.9922	
	O_1	0.4874	0.25	0.0745	
	O_2	0.3066	0.0384	0.7256	
FM	La	0.0465	0.25	0.9921	30.91
	O_1	0.4819	0.25	0.0769	
	O_2	0.2905	0.0406	0.7106	
AAF	La	0.0507	0.25	0.9920	30.87
	O_1	0.4856	0.25	0.0775	
	O_2	0.3030	0.0401	0.7202	

Table 6 Simultaneously optimised lattice constants in the orthorhombic LMO phase (a) and positions of ions inside the unit cell (b). E_{cut} = 600 eV, the ***k***-set is 4 2 4

(a)	a	b	c	Cohesive energy/eV cell^{-1}
FM	5.6209	7.9023	5.5381	30.93
AAF	5.7531	7.7214	5.5587	30.87
GAF	5.9431	7.6174	5.5511	30.82
CAF	5.5792	7.9557	5.4932	30.83

(b)	x	y	z
FM			
La	0.0427	0.25	0.9916
O_1	0.4840	0.25	0.0741
O_2	0.2897	0.0400	0.7112
AAF			
La	0.0512	0.25	0.9913
O_1	0.4844	0.25	0.0786
O_2	0.3019	0.0406	0.7194
GAF			
La	0.0643	0.25	0.9883
O_1	0.4832	0.25	0.0822
O_2	0.3193	0.0430	0.7199
CAF			
La	0.0409	0.25	0.9915
O_1	0.4859	0.25	0.0704
O_2	0.2921	0.0389	0.7112

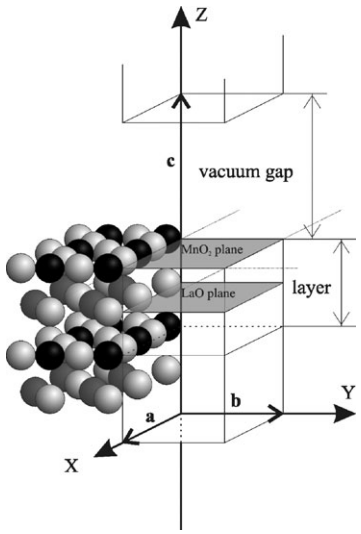

Fig. 2 Four-plane slab model with indication of supercell parameters (a, b, c) and vacuum gap.

moment of a polar slab, we used the dipole moment correction option incorporated into the VASP code.

The variations of the cut-off energy (from the default value of 269.9 eV up to 400 eV) and the vacuum gap (from 15.8 to 47.7 Å) as well as dipole moment corrections do not affect the main results. In order to reduce computational efforts, we used in most calculations the vacuum gap of 15.8 Å and the cut-off energy of 400 eV. The calculated total magnetic moment is nonzero for the AAF slabs; this is 0.9 μ_B, 0.65 μ_B, and 1.46 μ_B for the 4-, 8-, and 12-plane slabs, respectively. This is caused by different magnetic moments of Mn ions occupying different positions in the asymmetrical slab.

The relative atomic displacements for 8-plane slabs are summarised in Table 8. In agreement with bulk and surface energies, atomic displacements for the AAF and the FM configurations are also similar and strongly differ from those for the NM state. All Mn atoms are very moderately displaced from the perfect lattice sites, even on the MnO_2-terminated surface. Unlike Mn, La ions are strongly displaced towards nearest MnO_2-planes. Oxygen ions are strongly displaced inwards on the MnO_2-terminated surface, whereas they show slight displacement outwards on the LaO-terminated surface. Both terminations demonstrated considerable rumpling (*i.e.* relative displacement of Me, O atoms from the crystallographic MeO-plane). Unlike the AAF and FM, in NM slabs most of the atoms are displaced inwards which corresponds to a strong compression of the slab. This results from the fact that the optimised NM bulk lattice constant is considerably smaller than the experimental value of 3.95 Å.

To characterise the electronic density distribution, we calculated topological (Bader) charges, which are given in Table 9. In the bulk these are considerably smaller than the formal ionic charges (La^{3+}, Mn^{3+}, O^{2-}); this is caused by a covalent contribution to the chemical bonding between the Mn and O ions. MnO_2- and LaO-terminated surfaces demonstrate a quite different behaviour: the effective charges of the LaO termination remain very close to those in the bulk, whereas the effective charges of the MnO_2-plane are considerably reduced.

Table 7 Calculated surface energies for the unrelaxed and relaxed (E_{su} and E_s, respectively) surface energies (in eV) for LMO slabs of different thickness using PP-2 pseudopotentials; ***k***-points set Monkhorst–Pack 5 5 1; vacuum gap 15.8 Å, $a = b$ is the lattice vector parallel to the slab (in Å), experimental bulk value is 3.95 Å, different from this value means result of the optimisation, $E_{cut} = 400$ eV

No. of planes	$a = b$	Slab	E_{su}	E_s
4	3.95	NM	1.73	0.94
4	3.75	NM		0.91
4	3.95	AAF	1.68	0.74
4	3.83	AAF		0.67
4	3.95	FM	1.65	0.77
4	3.83	FM		0.70
6	3.95	NM	1.74	0.88
8	3.95	NM	1.74	0.80
8	3.77	NM		0.98
8	3.95	AAF	1.74	0.84
8	3.87	AAF		0.79
8	3.95	FM	1.68	0.84
8	3.86	FM		0.75
10	3.95	NM	1.74	0.72
12	3.95	NM	1.74	0.63
12	3.78	NM		0.99
12	3.95	AAF	1.78	0.89
12	3.88	AAF		0.86
12	3.95	FM	1.69	0.86
12	3.86	FM		0.74
14	3.95	NM	1.74	0.54

Table 8 The atomic relaxation for the NM, FM and AAF configurations of stoichiometric LMO 8-plane slab (displacements are along the z axis, in % of the bulk lattice constant of 3.95 Å). A positive sign means outward displacements from the slab center, whereas a negative one displacements towards the slab center

Plane		Relaxation		
		AAF	FM	NM
1	Mn	0.49	0.64	−12.02
	O2	−4.23	−3.95	−11.16
2	La	8.00	8.12	1.24
	O	−3.69	−2.57	−7.91
3	Mn	−0.61	0.19	−4.45
	O2	−4.32	−3.49	−6.19
4	La	5.34	5.69	3.18
	O	−0.93	−0.15	−1.31
5	Mn	−0.37	−0.33	−2.29
	O2	2.08	2.18	−0.63
6	La	−6.41	−6.11	−9.06
	O	−0.01	1.05	−4.27
7	Mn	−0.02	0.81	−6.11
	O2	1.32	1.91	−5.25
8	La	−9.83	−9.05	−16.68
	O	1.33	2.50	−5.80

Table 9 The effective Bader charges of atoms in the bulk and in 8-plane slab (in e), and their difference

Plane		Bulk	Surface	Difference
1	Mn	1.90	1.63	−0.27
	O_2	−1.28	−1.21	0.07
2	La	1.94	2.06	0.12
	O	−1.27	−1.15	0.12
3	Mn	1.90	1.77	−0.13
	O_2	−1.28	−1.23	0.05
4	La	1.94	2.05	0.11
	O	−1.27	−1.26	0.01
5	Mn	1.90	1.73	−0.17
	O_2	−1.28	−1.26	0.02
6	La	1.94	2.00	0.06
	O	−1.27	−1.20	0.07
7	Mn	1.90	1.79	−0.11
	O_2	−1.28	−1.34	−0.06
8	La	1.94	1.99	0.05
	O	−1.27	−1.33	−0.06

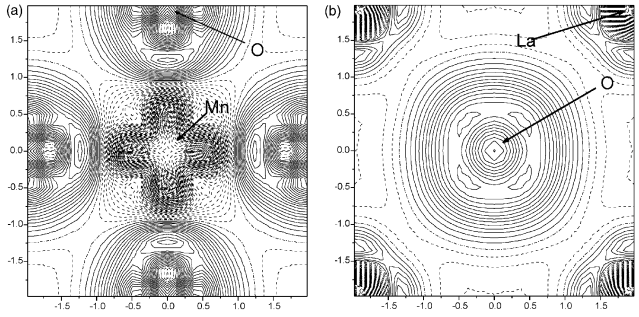

Fig. 3 The difference electron density maps for the top unrelaxed MnO (a) and LaO (b) planes calculated with respect to the superposition of atomic densities. Isodensity increment is 0.01 e Å^{-3}, full and dashed lines mean positive and negative electron densities, whereas dot–dash line is a zero level.

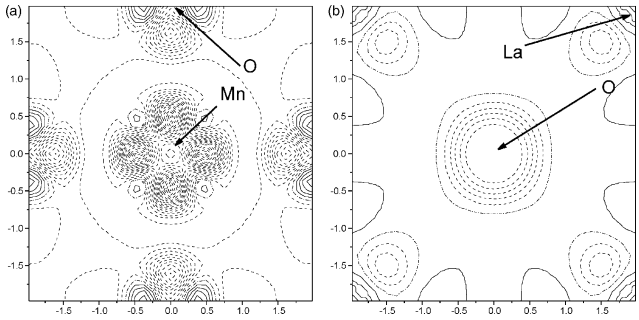

Fig. 4 The difference electron density maps for the top unrelaxed MnO (a) and LaO (b) planes calculated with respect to the superposition of self-consistent density for similar atoms in the bulk. Isodensity increment is 0.01 e Å^{-3}.

Very likely this is the result of increased covalent contribution to MnO chemical bonding on the surface. This is in line with our conclusion for the TiO_2-termination for the $SrTiO_3$ (001) surface.[11] The effective charges of the rest of the atoms inside the slab are close to the bulk values.

Lastly, Figs. 3 and 4 present the *difference electronic density maps* for the top unrelaxed MnO_2- and LaO- planes, calculated with respect to the superposition of atomic densities and the self-consistent density for similar atoms in the bulk plane. From these maps the following conclusions could be drawn: (a) a considerable covalent contribution in the Mn–O bonding takes place, (b) the effective charges on the MnO_2 surface are reduced as compared with those in the bulk.

Conclusions

Our calculations show that the surface energy of polar LMO (001) surface is smaller than that of the (110) surface. This indicates that the (001) surface could play an important role in the oxygen-related processes in fuel cells and other applications. For the first time we calculated the (001) surface relaxation which reduces the surface energy by a factor of about two. In the modelling of this surface, even at high temperatures when Mn spins are randomly distributed and no magnetic effects take place, one should not neglect the atomic spins but treat the slab in the AAF configuration where the total spin is close to zero. Despite the fact that the kinetic processes occur at high temperatures, our calculations give a good starting point for the modelling of molecular adsorption and diffusion on manganite surfaces. At the present time, we are studying effects of polar surface dipole moment compensation by means of surface vacancy introduction.

Acknowledgements

Authors are greatly indebted to F. Illas, J. Carrasco, N. Lopez, D. Fuks, E. Heifets, A. Bandura and J. Fleig for many stimulating discussions, as well as A. Arnaldsson and G. Henkelman for their help in calculating Bader charges. This study was supported by the German–Israeli Foundation (GIF project G-703.41.10/2001).

References

1 J. Fleig, K. D. Kreuer and J. Maier, in *Handbook of Advanced Ceramics*, Elsevier, Singapore, 2003, p. 57.
2 Y.-S. Su, T. A. Kaplan, S. D. Mahanti and J. F. Harrison, *Phys. Rev.*, 2000, **B 61**, 1324.
3 M. Nicastro and C. H. Patterson, *Phys. Rev.*, 2002, **B65**, 205111.
4 P. Pavindra, A. Kjekshus, H. fjellvag, A. Delin and O. Eriksson, *Phys. Rev.*, 2002, **B65**, 64445.
5 N. N. Kovaleva, J. L. Gavartin, A. L. Shluger, A. V. Boris and A. M. Stoneham, *J. Exp. Theor. Phys.*, 2002, **94**, 178.
6 (*a*) A. Filipetti and W. E. Pickett, *Phys. Rev. Lett.*, 1999, **83**, 4184; (*b*) A. Filipetti and W. E. Pickett, *Phys. Rev.*, 2000, **B62**, 11571.
7 E. A. Kotomin, E. Heifets, J. Maier and W. A. Goddard III, *Phys. Chem. Chem. Phys.*, 2003, **5**, 4180.
8 E. Heifets, R. A. Evarestov, E. A. Kotomin, S. Dorfman and J. Maier, *Sens. Actuators, B*, 2004, **B100**, 81.
9 E. A. Kotomin, E. Heifets, S. Dorfman, D. Fuks, A. Gordon and J. Maier, *Surf. Sci.*, 2004, **566**, 231.
10 R. A. Evarestov, E. A. Kotomin, E. Heifets, J. Maier and G. Borstel, *Solid State Commun.*, 2003, **127**, 367.
11 R. A. Evarestov, E. A. Kotomin, D. Fuks, J. Felsteiner and J. Maier, *Appl. Surf. Sci.*, 2004, **238**, 457.
12 D. Munoz, N. M. Harrison and F. Illas, *Phys. Rev.*, 2004, **B69**, 85115.
13 (*a*) G. Kresse and J. Hafner, *Phys. Rev.*, 1993, **B48**(13), 115; (*b*) G. Kresse and J. Hafner, *Phys. Rev.*, 1994, **B49**, 14521.
14 G. Kresse and J. Furthmüller, *VASP, the Guide*, University of Vienna, Austria, 2003.
15 J. Rodrýguez-Carvajal, M. Hennion, F. Moussa and A. H. Moudden, *Phys. Rev.*, 1998, **B57**, 3190.
16 K. Burke, J. P. Perdew and Y. Wang, in *Electronic Density Functional Theory: Recent Progress and New Directions*, ed. J. F. Dobson, G. Vignale and M. P. Das, Plenum, New York, 1998.
17 H. J. Monkhorst and J. D. Pack, *Phys. Rev.*, 1976, **B13**, 5188.

